11. Clayton, R. N. Oxygen isotopes in meteorites. *Annu. Rev. Earth Planet. Sci.* **21,** 115–149 (1993).
12. Lewis, R. S., Anders, E., Wright, I. P., Norris, S. J. & Pillinger, C. T. Isotopically anomalous nitrogen in primitive meteorites. *Nature* **305,** 767–771 (1983).
13. Thiemens, M. H. & Heidenreich, J. E. III The mass-independent fractionation of oxygen: A novel isotope effect and its possible cosmochemical implications. *Science* **219,** 1073–1075 (1983).
14. Clayton, R. N. Self-shielding in the solar nebula. *Nature* **415,** 860–861 (2002).
15. Lee, T., Shu, F. H., Shang, H., Glassgold, A. E. & Rehm, K. E. Protostellar cosmic rays and extinct radioactivities in meteorites. *Astrophys. J.* **506,** 898–912 (1998).
16. Shukolyukov, A. & Lugmair, G. W. Manganese-chromium isotope systematics of Ivuna, Kainsaz and other carbonaceous chondrites. *Lunar Planet. Sci.* **XXXIV,** 1279 (2003).
17. Niederer, F. R., Papanastassiou, D. A. & Wasserburg, G. J. Absolute isotopic abundances of Ti in meteorites. *Geochim. Cosmochim. Acta* **49,** 835–851 (1985).
18. Dauphas, N., Marty, B. & Reisberg, L. Inference on terrestrial genesis from molybdenum isotope systematics. *Geophys. Res. Lett.* **29,** 1084 (2002).
19. Becker, H. & Walker, R. J. Ruthenium isotopic composition of terrestrial materials, iron meteorites and chondrites. *Lunar Planet. Sci.* **XXXIII,** 1018 (2002).
20. Becker, H. & Walker, R. J. In search of extant Tc in the early solar system: ^{98}Ru and ^{99}Ru abundances in iron meteorites and chondrites. *Chem. Geol.* **196,** 43–56 (2003).
21. Schönbächler, M., Lee, D.-C., Halliday, A. N. & Rehkämper, M. Uniformity of zirconium isotopic compositions in the inner solar system. *Lunar Planet. Sci.* **XXXIII,** 1283 (2002).
22. Pernicka, E. & Wasson, J. T. Ru, Re, Os, Pt and Au in iron meteorites. *Geochim. Cosmochim. Acta* **51,** 1717–1726 (1987).
23. Becker, H., Morgan, J. W., Walker, R. J., MacPherson, G. J. & Grossman, J. N. Rhenium-osmium systematics of calcium-aluminium-rich inclusions in carbonaceous chondrites. *Geochim. Cosmochim. Acta* **65,** 3379–3390 (2001).
24. McCulloch, M. T. & Wasserburg, G. J. Barium and neodymium isotopic anomalies in the Allende meteorite. *Astrophys. J.* **220,** L15–L19 (1978).
25. Shu, F. H., Shang, H. & Lee, T. Toward an astrophysical theory of chondrites. *Science* **271,** 1545–1552 (1996).
26. Nier, A. O. A redetermination of the relative abundances of the isotopes of carbon, nitrogen, oxygen, argon and potassium. *Phys. Rev.* **77,** 789–793 (1950).
27. Qi Lu & Masuda, A. The isotopic composition and atomic weight of molybdenum. *Int. J. Mass Spectrom. Ion Proc.* **130,** 65–72 (1994).
28. Russell, W. A., Papanastassiou, D. A. & Tombrello, T. A. Ca isotope fractionation on the Earth and other solar system materials. *Geochim. Cosmochim. Acta* **42,** 1075–1090 (1978).

Acknowledgements We thank R. Clarke and G. MacPherson for providing the meteorite samples, N. Dauphas, H. Palme, D. Papanastassiou, A. Pietruszka and Q. Yin for discussions, and P. Tomascak for comments on the manuscript and technical support in the laboratory. Comments by S. Jacobsen have improved the presentation of various issues in this manuscript.

Competing interests statement The authors declare that they have no competing financial interests.

Correspondence and requests for materials should be addressed to H.B. (hbecker@geol.umd.edu).

Quantum dynamics of a single vortex

A. Wallraff*, A. Lukashenko, J. Lisenfeld, A. Kemp, M. V. Fistul, Y. Koval & A. V. Ustinov

Physikalisches Institut III, Universität Erlangen-Nürnberg, D-91058 Erlangen, Germany

* Present address: Department of Applied Physics, Yale University, New Haven, Connecticut 06520, USA

Vortices occur naturally in a wide range of gases and fluids, from macroscopic to microscopic scales. In Bose–Einstein condensates of dilute atomic gases[1], superfluid helium[2] and superconductors, the existence of vortices is a consequence of the quantum nature of the system. Quantized vortices of supercurrent[3] are generated by magnetic flux penetrating the material, and play a key role in determining the material properties[4] and the performance of superconductor-based devices[5,6]. At high temperatures the dynamics of such vortices are essentially classical, while at low temperatures previous experiments have suggested collective quantum dynamics[7,8]. However, the question of whether vortex tunnelling occurs at low temperatures has been addressed only for large collections of vortices. Here we study the quantum dynamics of an individual vortex in a superconducting Josephson junction. By measuring the statistics of the vortex escape from a controllable pinning potential, we demonstrate the existence of quantized levels of the vortex energy within the trapping potential well and quantum tunnelling of the vortex through the pinning barrier.

The object that we have studied in our experiments is a vortex of electric current with a spatial extent of several tens of micrometres formed in a long superconducting tunnel junction. The electrodynamics of such a Josephson junction is governed by the phase difference ϕ between the macroscopic wavefunctions describing the superconducting condensate in the two electrodes[9]. It is a well established fact that the variable ϕ does display macroscopic quantum properties in point-like junctions at very low temperatures[10,11]. Such macroscopic quantum phenomena are currently exploited for quantum information processing[12] using superconducting devices[10,13–17]. In extended one- or two-dimensional Josephson junction systems, quantum tunnelling in real space is to be expected for superconducting vortices, which are particle-like collective excitations of the phase difference ϕ. Collective nonlinear excitations such as the vortex considered here are ubiquitous in solid state systems (for example, domain walls), biological systems (such as waves on membranes), and have even been considered as model systems in particle physics. The small value of the expected mass of the vortex studied here suggests that quantum effects are likely to occur with vortices at low temperatures. Dissipative vortex tunnelling has been put forward as a reason for the non-vanishing relaxation rate of the magnetization in type-II superconductors as the temperature T is lowered towards zero. However, the quantum vortex creep model[8], which was suggested as an explanation for this behaviour, faced orders-of-magnitude discrepancies with experimental data[18]. Alternative classical explanations have been suggested more recently to explain the low-temperature relaxation[19]. Nonetheless, macroscopic quantum tunnelling was observed for states with many vortices in discrete arrays of small Josephson junctions[20,21]. For typical arrays, the calculated vortex mass is about 500 times smaller than the electron mass[7]. All previous research in this area has focused on the collective behaviour of a large number of vortices. Until now there had been no direct experimental observation of tunnelling events of individual vortices.

Among many different vortex structures in superconductors, there is a rather special type of vortex in long Josephson junctions. These vortices have the characteristics of solitons—nonlinear waves that preserve their shape with time and propagate as ballistic particles[22]. These vortices are distinct from Abrikosov vortices in type-II superconductors, as they have no normal core and thus move with very low damping. In contrast to vortices in Josephson arrays[7], solitons in uniform long junctions do not generate any radiation during their motion, and are well decoupled from other electromagnetic excitations in these systems. The quantum tunnelling of Josephson vortices in long junctions has been predicted theoretically[23,24]. Here we present experimental observations of this effect.

We probe the quantum properties of a single Josephson vortex in a current-biased annular junction subject to an in-plane magnetic field H (Fig. 1c inset). The junction (of diameter $d = 100\,\mu$m and width $w = 0.5\,\mu$m) is etched from a sputtered Nb/AlO_x/Nb thin-film trilayer which is patterned using electron-beam lithography[25]. A photograph of the sample taken using an optical microscope is shown in Fig. 1a. Initially the vortex is topologically trapped in the junction by cooling the sample in a small perpendicular magnetic field H_{tr}, which is generated using a separate pair of coils, the axis of which is perpendicular to the junction plane (Fig. 1b). A single vortex in an annular junction subject to an in-plane field behaves as a particle[26] in a tilted washboard potential[27,28]. The component of the potential periodic in the vortex coordinate Θ is due to the interaction $\mu \cdot H \propto \cos\Theta$ of the vortex magnetic moment μ with the external magnetic field H (Fig. 1c). The tilt of the potential is proportional to the Lorentz force acting on the vortex which is induced by the bias current I applied to the junction. The vortex

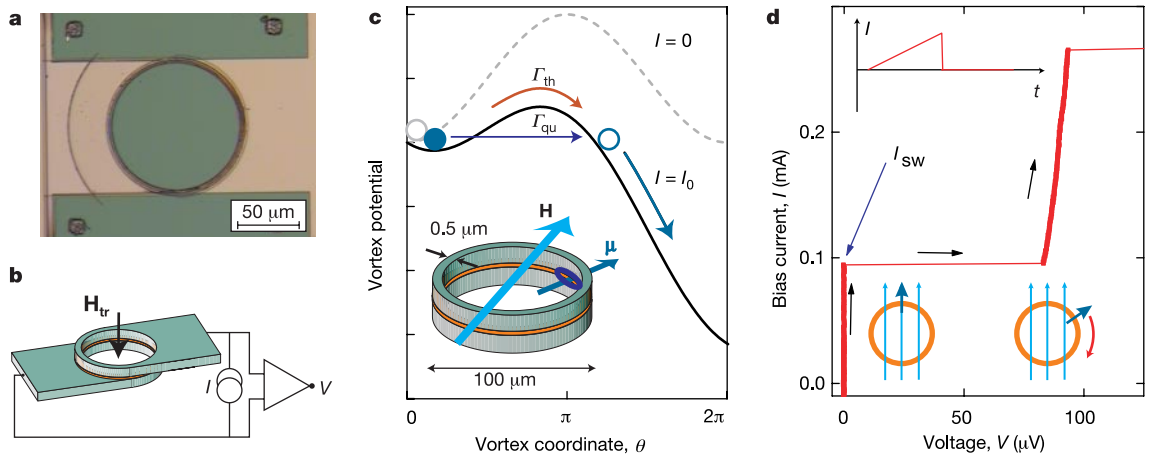

Figure 1 Sample, vortex potential and switching current measurement. **a**, Photograph of the sample taken with an optical microscope. **b**, Sketch of bias lead configuration and direction of trapping field H_{tr}. We use a bias lead geometry which minimizes self field effects[34] and apply the magnetic field H generating the vortex potential in the plane of the junction but perpendicular to the bias leads. In this case, the vortex is depinned in a location along the junction where self fields are minimal. **c**, A vortex with magnetic moment μ trapped in an annular Josephson junction subject to an in-plane external magnetic field H. The junction width and diameter are indicated (see inset). The resulting vortex potential at zero bias current I (dashed line) and at finite bias I_0 (solid line) is plotted versus the vortex coordinate Θ in the annulus. Thermal and quantum escape of the vortex at rates Γ_{th} and Γ_{qu}, respectively are indicated. **d**, Current–voltage characteristic showing the vortex depinning from the field induced potential at a random value of bias I_{sw} when ramping up the bias current at a constant rate in a saw-tooth pattern (see upper inset). The transition of a pinned vortex state to a running vortex state is associated with a voltage appearing across the junction which is proportional to the vortex velocity (see lower insets). In experiment, the bias current is switched off immediately after a voltage is detected.

may escape from a well in the tilted potential by a thermally activated process or by quantum tunnelling. At low temperatures thermal activation is exponentially suppressed, and the escape occurs by quantum tunnelling. This process is identified by measuring the temperature dependence of the distribution P of depinning currents I_{sw} (refs 29, 30) of the vortex trapped in the junction. The $P(I_{sw})$ distributions are recorded by repeatedly ramping up the bias current at a constant rate $\dot{I}$ and recording the statistics of the current I_{sw} at which the vortex escapes from the well, which is associated with a switching of the junction from its zero-voltage state to a finite-voltage state (Fig. 1d). Our measurement technique and set-up have been tested and calibrated[30,31] in experiments on macroscopic quantum tunnelling of the phase in small Josephson junctions[11].

The bias current I_p at which vortex tunnelling occurs with the highest probability (for a given bias current ramp rate) is found—as expected[27,28]—to be proportional to the applied magnetic field (see below). This indicates that the shape of the potential is controlled in our experiment by both field and bias current. The effect of the bias-current-induced self magnetic field on the vortex potential has been minimized by using an appropriate bias lead configuration and field direction (Fig. 1b).

To search for quantum tunnelling of the vortex, the temperature dependence of the switching current distribution $P(I_{sw})$ has been measured. In Fig. 2a such distributions are shown for a magnetic field of $H = 0.9$ Oe applied in the plane of the junction. It is clearly observed that the distribution width σ decreases with temperature and then saturates at low T. In Fig. 2b, σ is plotted versus temperature on a double logarithmic scale for two different values of field. At high temperatures, the distribution width is temperature dependent, indicating the thermally activated escape of the vortex from the well. In the high temperature limit σ is, to a good approximation, proportional to $T^{2/3}$ as expected for a thermally activated escape of a particle from a washboard potential close to critical bias. The distribution width σ saturates at a temperature of about 100 mK. This behaviour indicates the cross-over of the vortex escape process from thermal activation to quantum tunnelling. At temperatures below 100 mK, σ is constant and the escape is dominated by quantum tunnelling. As expected, the cross-over temperature T^* is dependent on magnetic field, but only rather weakly. We attribute this observation to the fact that the vortex may change its shape when traversing the barrier during the escape process. This aspect can not be captured in the single-particle model[26,27], but rather is a consequence of the fact that the vortex is a collective excitation.

To probe the energy levels of the vortex in the potential well, we have measured the vortex escape in the presence of microwave radiation, using spectroscopic techniques which we have extensively tested on small Josephson junctions[31]. At low temperatures and in the absence of microwave radiation, the vortex tunnels out of the ground state of the potential well into the continuum. The occupation of excited states is exponentially small, if the level separation is larger than the temperature. By irradiating the sample with microwaves, the vortex can be excited resonantly from the ground state to the first excited state (Fig. 3b inset). In this case, we observe a double peak structure in the switching current distribution (Fig. 3a). The peak at higher bias current is due to the tunnelling of the vortex from the ground state, whereas the peak at lower bias current corresponds to the tunnelling out of the first excited state.

The energy level separation scales both with bias current and applied magnetic field. To investigate this property, we have spectroscopically determined the separation between the ground and the first excited state by varying the microwave frequency and the magnetic field. For each value of the magnetic field, we have determined the resonance current I_r (see Fig. 3a) for a few different microwave frequencies ν. In Fig. 3b, the applied microwave frequency ν is plotted versus the resonance current I_r normalized by the depinning current $I_c(H)$ at that field in absence of microwaves and fluctuations. It is observed that all data points show the characteristic scaling of the energy level separation $\Delta E_{01}/h$ with the bias current as $\nu_{01}(H, I) = \nu_{01}(H, I = 0)(1 - (I/I_c(H))^2)^{1/4}$, as expected for the tilted washboard potential. The data at each field are fitted to this dependence using the characteristic frequency $\nu_{01}(H, I = 0)$ of vortex oscillations at zero current and the depin-

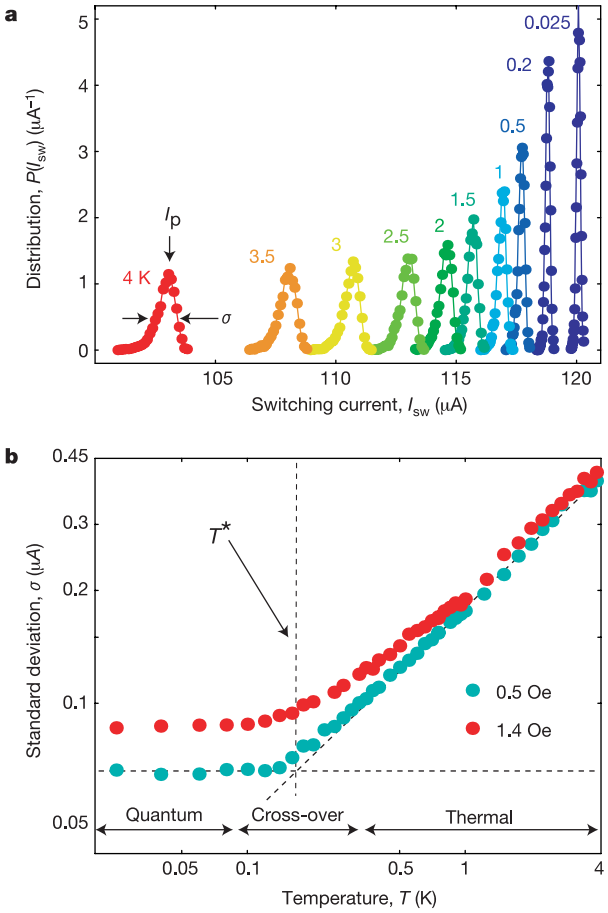

Figure 2 Thermal activation and quantum tunnelling. **a**, Switching current distributions $P(I_{sw})$ at magnetic field $H = 0.9$ Oe for bath temperatures T between 4.0 K and 25 mK. **b**, Standard deviation σ of $P(I_{sw})$ versus T for two values of field, indicating the cross-over in the vortex escape process from thermal activation to quantum tunnelling. The cross-over temperature range around T^* is indicated. We have carefully verified experimentally that the saturation of the distribution width with temperature is not induced by excess noise or heating of the sample. The resolution of our measurement set-up[30] is factor of 3 to 4 larger than the most narrow distribution widths measured in these experiments.

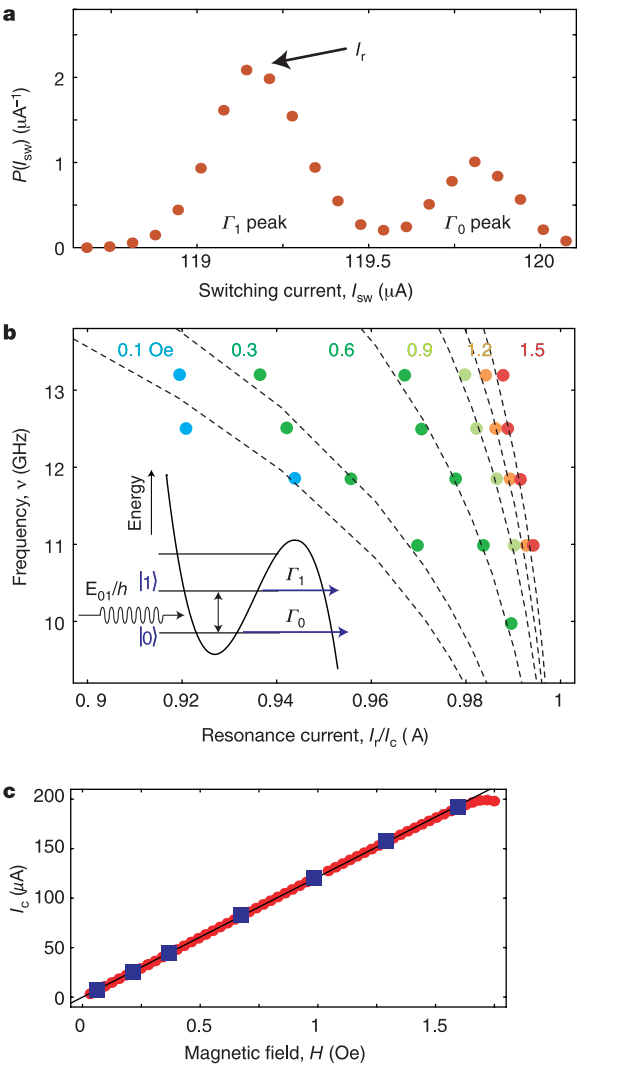

Figure 3 Vortex energy levels. **a**, $P(I_{sw})$ distribution at $H = 0.6$ Oe in the presence of microwave radiation of $\nu = 11$ GHz at $T = 25$ mK. The resonance current I_r at which tunnelling from the first excited state is most probable is indicated. **b**, Microwave frequency ν versus normalized resonance current $I_r/I_c(H)$ for magnetic fields H between 0.1 and 1.5 Oe. Dashed curves are fits to $\nu_{01}(H, I = 0)(1 - (I/I_c(H))^2)^{1/4}$. In the inset is indicated the tunnelling from the ground state at rate Γ_0 and from the first excited state populated by resonant microwave radiation at rate Γ_1. **c**, Critical current I_c extracted from microwave spectroscopy (filled squares), most probable switching current I_p at $T = 25$ mK in absence of microwaves (solid circles) and fit (solid line) versus magnetic field H.

ning current $I_c(H)$ as fitting parameters, see dashed lines in Fig. 3b. The resonance frequency $\nu_{01}(H, I = 0)$ and the depinning current $I_c(H)$ in absence of fluctuations have been determined from the fit. As expected, the energy level separation ΔE_{01} increases with field and the depinning current I_c as determined from the spectroscopic data is linear in the field, see Fig. 3c, which is in excellent agreement with the current I_p measured directly in absence of microwaves.

From the resonance frequency at a given bias current we can estimate the cross-over temperature, which in the limit of small damping is given by $T^* \approx h\nu_{01}(H, I)/2\pi k_B$. Thus we can compare the cross-over temperature extracted from the temperature dependence of the switching current distributions to the predictions based on the data extracted from spectroscopic measurements. For $\nu_{01}(H, I)$ between 10 and 13 GHz we find a value of T^* between approximately 75 and 100 mK, which is consistent with the measured saturation temperature in Fig. 2.

The quantum dynamics of vortices are important for evaluating the properties of superconducting materials and devices at low temperatures. Similar effects to those observed here in a superconductor may well be observable in atomic Bose–Einstein condensates or in superfluid helium. The results of our experiments may directly open a path towards quantum computation[12] using Josephson vortices in long junctions as qubits[32,33]. □

Received 31 March; accepted 17 June 2003; doi:10.1038/nature01826.

1. Abo-Shaeer, J. R., Raman, C., Vogels, J. M. & Ketterle, W. Observation of vortex lattices in Bose-Einstein condensates. *Science* **292,** 476–479 (2001).
2. Blaauwgeers, R. *et al.* Double-quantum vortex in superfluid ^{3}He-A. *Nature* **404,** 471–473 (2000).
3. Huebener, R. P. *Magnetic Flux Structures in Superconductors* (Springer, Berlin, 2001).
4. Bugoslavsky, Y., Perkins, G. K., Qi, X., Cohen, L. F. & Caplin, A. D. Vortex dynamics in superconducting MgB_2 and prospects for applications. *Nature* **410,** 563–565 (2001).
5. Nori, F. & Savel'ev, S. Experimentally realizable devices for controlling the motion of magnetic flux quanta in anisotropic superconductors. *Nature Mater.* **1,** 179–184 (2002).
6. Lee, C.-S., Janko, B., Derenyi, I. & Barabesi, A.-L. Reducing the vortex density in superconductors using the ratchet effect. *Nature* **400,** 337–340 (1999).
7. Fazio, R. & van der Zant, H. J. S. Quantum phase transitions and vortex dynamics in superconducting networks. *Phys. Rep.* **355,** 235–334 (2001).
8. Blatter, G., Feigel'man, M. V., Geshkenbein, A. I. & Vinokur, V. M. Vortices in high-temperature superconductors. *Rev. Mod. Phys.* **66,** 1125–1388 (1994).
9. Tinkham, M. *Introduction to Superconductivity* (McGraw-Hill International Editions, New York, 1996).

10. Clarke, J., Cleland, A. N., Devoret, M. H., Esteve, D. & Martinis, J. M. Quantum mechanics of a macroscopic variable: The phase difference of a Josephson junction. *Science* **239,** 992–997 (1988).
11. Devoret, M. H. *et al.* in *Quantum Tunneling in Condensed Media*, (eds Kagan, Yu. & Leggett, A. J.) (North-Holland, Amsterdam, 1992).
12. Bennett, C. H. & DiVincenzo, D. P. Quantum information and computation. *Nature* **404,** 247–255 (2000).
13. Nakamura, Y., Pashkin, Y. A. & Tsai, J. S. Coherent control of macroscopic quantum states in a single-Cooper-pair box. *Nature* **398,** 786–788 (1999).
14. Friedman, J. R., Patel, V., Chen, W., Tolpygo, S. K. & Lukens, J. E. Quantum superposition of distinct macroscopic states. *Nature* **406,** 43–46 (2000).
15. van der Wal, C. H. *et al.* Quantum superposition of macroscopic persistent-current states. *Science* **290,** 773–777 (2000).
16. Pashkin, Y. A. *et al.* Quantum oscillations in two coupled charge qubits. *Nature* **421,** 823–826 (2003).
17. Chiorescu, I., Nakmura, Y., Harmans, C. J. P. M. & Mooji, J. E. Coherent quantum dynamics of a superconducting flux qubit. *Science* **299,** 1869–1871 (2003).
18. Hoekstra, H. F. T. *et al.* General features of quantum creep in high- T_c superconductors. *Phys. Rev. Lett.* **80,** 4293–4296 (1998).
19. Nicodemi, M. & Jensen, H. J. Creep of superconducting vortices in the limit of vanishing temperature: A fingerprint of off-equilibrium dynamics. *Phys. Rev. Lett.* **86,** 4378–4381 (2001).
20. van der Zant, H. S. J., Fritschy, J. F. C., Orlando, T. P. & Mooij, J. E. Dynamics of vortices in underdamped Josephson-junction arrays. *Phys. Rev. Lett.* **66,** 531–2534 (1991).
21. Tighe, T. S., Johnson, A. T. & Tinkham, M. Vortex motion in two-dimensional arrays of small, underdamped Josephson junctions. *Phys. Rev. B* **44,** 10286–10290 (1991).
22. Ustinov, A. V. Solitons in Josephson junctions. *Physica D* **123,** 315–329 (1998).
23. Kato, T. & Imada, M. Macroscopic quantum tunneling of a fluxon in a long Josephson junction. *J. Phys. Soc. Jpn* **65,** 2963–2975 (1996).
24. Shnirman, A., Ben-Jacob, E. & Malomed, B. A. Tunneling and resonant tunneling of fluxons in a long Josephson junction. *Phys. Rev. B* **56,** 14677–14685 (1997).
25. Koval, Y. *et al.* Narrow long Josephson junctions. *IEEE Trans. Appl. Supercond.* **9,** 3957–3961 (1999).
26. McLaughlin, D. W. & Scott, A. C. Perturbation analysis of fluxon dynamics. *Phys. Rev. A* **18,** 1652–1980 (1978).
27. Grønbech-Jensen, N., Lomdahl, P. & Samuelsen, M. Phase locking of long annular Josephson junctions coupled to an external rf magnetic field. *Phys. Lett. A* **154,** 14–18 (1991).
28. Ustinov, A. V. & Thyssen, N. Experimental study of fluxon dynamics in a harmonic potential well. *J. Low Temp. Phys.* **106,** 193–200 (1997).
29. Fulton, T. A. & Dunkleberger, L. N. Lifetime of the zero-voltage state in Josephson tunnel junctions. *Phys. Rev. B* **9,** 4760–4768 (1974).
30. Wallraff, A. *et al.* Switching current measurements of large area Josephson tunnel junctions. *Rev. Sci. Instrum* **74,** 3740–3748 (2003).
31. Wallraff, A., Duty, T., Lukashenko, A. & Ustinov, A. V. Multi-photon transitions between energy levels in a current-biased Josephson tunnel junction. *Phys. Rev. Lett.* **90,** 037003 (2003).
32. Wallraff, A., Koval, Y., Levitchev, M., Fistul, M. V. & Ustinov, A. V. Annular long Josephson junctions in a magnetic field: Engineering and probing the fluxon potential. *J. Low Temp. Phys.* **118,** 543–553 (2000).
33. Kemp, A., Wallraff, A. & Ustinov, A. V. Josephson vortex qubit: Design, preparation and read-out. *Phys. Status Solidi B* **233,** 472–481 (2002).
34. Martucciello, N. *et al.* Fluxon dynamics in long annular Josephson tunnel junctions. *Phys. Rev. B* **57,** 5444–5449 (1998).

Acknowledgements We thank G. Blatter, T. Kato, G. Schön and S. Shnirman for discussions. This work was supported in part by the Deutsche Forschungsgemeinschaft (DFG).

Competing interests statement The authors declare that they have no competing financial interests.

Correspondence and requests for materials should be addressed to A.W. (andreas.wallraff@yale.edu).

Efficient bulk heterojunction photovoltaic cells using small-molecular-weight organic thin films

Peter Peumans, Soichi Uchida & Stephen R. Forrest

Center for Photonics and Optoelectronic Materials (POEM), Department of Electrical Engineering and the Princeton Materials Institute, Princeton University, Princeton, New Jersey 08544, USA

The power conversion efficiency of small-molecular-weight and polymer organic photovoltaic cells has increased steadily over the past decade. This progress is chiefly attributable to the introduction of the donor–acceptor heterojunction[1,2] that functions as a dissociation site for the strongly bound photogenerated excitons. Further progress was realized in polymer devices through use of blends of the donor and acceptor materials[3–5]: phase separation during spin-coating leads to a bulk heterojunction that removes the exciton diffusion bottleneck by creating an interpenetrating network of the donor and acceptor materials. The realization of bulk heterojunctions using mixtures of vacuum-deposited small-molecular-weight materials has, on the other hand, posed elusive: phase separation induced by elevating the substrate temperature inevitably leads to a significant roughening of the film surface and to short-circuited devices. Here, we demonstrate that the use of a metal cap to confine the organic materials during annealing prevents the formation of a rough surface morphology while allowing for the formation of an interpenetrating donor–acceptor network. This method results in a power conversion efficiency 50 per cent higher than the best values reported for comparable bilayer devices, suggesting that this strained annealing process could allow for the formation of low-cost and high-efficiency thin film organic solar cells based on vacuum-deposited small-molecular-weight organic materials.

The external quantum efficiency of a photovoltaic cell based on exciton dissociation at a donor–acceptor interface is[6] $\eta_{EQE} = \eta_A \times \eta_{ED} \times \eta_{CC}$. Here, η_A is the absorption efficiency. The exciton diffusion efficiency, η_{ED}, is the fraction of photogenerated excitons that reaches a donor–acceptor interface before recombining. The carrier collection efficiency, η_{CC}, is the probability that a free carrier, generated at a donor–acceptor interface by dissociation of an exciton, reaches its corresponding electrode. Typically, in bilayer donor–acceptor photovoltaic cells with a total thickness, L, of the order of the optical absorption length, L_A, we have $\eta_A = 1 - \exp(-L/L_A) > 50\%$ if optical interference effects are ignored, and $\eta_{CC} \approx 100\%$. However, since the exciton diffusion length (L_D) is typically an order of magnitude smaller than L_A, a large fraction of the photogenerated excitons remains unused for photocurrent generation[6] (Fig. 1a), limiting η_{EQE} and hence the power conversion efficiency, η_P, of this type of planar junction cell.

In polymer photovoltaic cells, the exciton diffusion bottleneck has been removed through the introduction of bulk heterojunctions[4,5] (Fig. 1b). In a bulk heterojunction, the donor–acceptor interface is highly folded such that photogenerated excitons find an interface within a distance L_D of their generation site. Currently, state-of-the-art bulk heterojunction polymer photovoltaic cells have power conversion efficiencies of up to 3.5% (refs 7–9). The bulk heterojunction is fabricated by spin-coating a mixture of the donor and acceptor materials. During spin coating and solvent evaporation, the donor and acceptor materials phase separate, creating an intricate interpenetrating network.

Attempts to achieve a bulk heterojunction through codeposition of the donor and acceptor materials yielded devices with η_P values falling short of those achievable in optimized bilayer cells using the same materials[10–16]. Strong quenching of the photoluminescence in mixed materials indicates that $\eta_{ED} \approx 100\%$. Therefore, the low efficiencies are attributed to poor charge transport, resulting in a low η_{CC} (Fig. 1c). If charge collection is assisted by the application of an external voltage, a high η_{EQE} can be obtained[17].

Growth of mixed layers at elevated substrate temperatures leads to phase separation and the appearance of crystalline domains. However, this increase in crystallinity and possibly larger L_D comes at the cost of an increased film roughness[13,18]. The high density of pinholes leads to short circuits and makes device fabrication impractical. The same problem occurs when mixed-layer films are annealed post-deposition to induce phase separation.

Here, we present a method for the fabrication of bulk heterojunctions in small-molecule systems based on annealing mixed-layer films in a confined geometry. In this case, the devices are completed with a ~1,000-Å-thick metal cathode, and then subsequently annealed. The metal cathode stresses the organic film during annealing, preventing morphological relaxation and the concomitant formation of a high density of pinholes, while

